ELSEVIER

Journal of Alloys and Compounds 293–295 (1999) 583–592

Journal of ALLOYS AND COMPOUNDS

A review on the development of AB_2-type Zr-based Laves phase hydrogen storage alloys for Ni–MH rechargeable batteries in the Korea Advanced Institute of Science and Technology

Dong-Myung Kim, Kuk-Jin Jang, Jai-Young Lee*

Department of Materials Science and Engineering, Korea Advanced Institute of Science and Technology, 373-1 Kusong-dong, Yusong-gu, Taejon, South Korea

Abstract

Our second endeavor was concentrated on improving the shortcomings of Zr-based alloys for commercialization, i.e., poor activation property and low rate capability. To improve the activation property of AB_2-type $Zr_{0.7}Ti_{0.3}Cr_{0.3}Mn_{0.3}V_{0.4}Ni_{1.0}$ alloy electrode, a new activation process called hot-charging treatment has been developed. In this new process, alloy electrodes were immersed in KOH solution and charged simultaneously at various solution temperatures and charging current densities for various treatment times. It was found that the activation property of this alloy electrode are greatly improved after the hot-charging treatment, and furthermore the electrode treated at 80°C and 50 mA g^{-1} for 8 h was fully activated after the first cycle. Extensive work has been carried out on the development of the Zr-based Laves phase alloy with high capacity and especially with high rate capability for electrochemical application. After careful alloy design of $ZrMn_2$-based Laves phase alloys through varying their stoichiometry by substituting or adding some alloying elements, $Zr_{0.9}Ti_{0.1}(Mn_{0.7}V_{0.5}Ni_{1.4})_{0.92}$ alloy with high capacity and high rate capability was developed consequently. This alloy has the design capacity of 394 mAh g^{-1}, i.e., 35% higher capacity than that of commercialized AB_5-type alloys, at the discharge rate of 0.25C and shows a very high rate capability. It is therefore believed that the commercialization of Zr-based alloy for Ni–MH rechargeable batteries is coming soon.

Keywords: Activation; Hot-charging; Rate capability; Reaction surface area; Over-stoichiometry

1. Introduction

Nickel–metal hydride (Ni–MH) batteries using a proper hydrogen storage alloy as a negative electrode has been recognized as a better substitute than Ni–Cd batteries because of their higher energy density and better environmentally friendly nature. Among hydrogen storage alloys, AB_5-type alloys are commercially more favored and better developed as negative electrode materials than others. In 1996, high capacity Ni–MH rechargeable batteries were reported, with higher volumetric energy density than Li-ion batteries. More improvements are expected if AB_2-type alloys, which have higher hydrogen storage capacity than AB_5-type alloya, are to be commercialized. In particular, Zr-based AB_2-type alloys are very promising due to their higher hydrogen storage capacities and longer cycle life than those of commercial AB_5-type alloys, especially if their poor activation property and relatively low rate capacity are improved.

In this article, the result of studies in the Korea Advanced Institute of Science and Technology, on developing on AB_2-type Zr-based hydrogen storage alloys with high rate capacity and on improving their activation property are summarized.

2. A development of a Zr-based hydrogen storage alloy with high rate capability and high capacity

In general, most of Zr-based Laves phase MHs are disappointing regarding rate capacity compared with that of the commercialized AB_5-type alloys. Therefore, many researches have been focused on developing Zr-based alloys with high capacity and especially with high rate capacity for electrochemical application. However, there are few remarkable results on improving the rate capability.

In this section, the results and discussion of extensive research on developing the Zr-based Laves phase alloys

*Corresponding author.

0925-8388/99/$ – see front matter
PII: S0925-8388(99)00414-4

with high capacity and especially with rate capacity for practical application are reported.

2.1. Selection of starting material for developing Zr-based Laves phase alloys

The $ZrMn_2$ compound has a large hydrogen storage capacity of about 1.5 wt.%, but it cannot be discharged in KOH solution itself. After careful design of the $ZrMn_2$-based alloy to have suitable hydrogen equilibrium pressure and to achieve higher discharging capacity in KOH solution, $ZrMn_{0.5}V_{0.5}Ni_{1.4}$ alloy reveal rather good properties in view of hydrogen storage capacity of about 1.5 wt.% at hydrogen equilibrium pressure ranges of application and electrochemical discharge capacity of about 315 mAh g^{-1} (Fig. 1)

2.2. Major factor controlling the rate capacity of Zr-based Laves phase alloy

In order to optimize the composition of these quaternary alloy with high capacity and high rate capacity, the major factor affecting the discharge capacity and the rate capacity of the alloy system should be determined. Therefore, in our previous work [1], the hydrogen storage performance, i.e., the pressure–composition–temperature (PCT) curve, and discharge characteristics, i.e., discharge capacity and rate capability, of $ZrMn_{0.5}V_{0.5}Ni_{1.4+y}$ (y=0.0, 0.2, 0.4 and 0.6) alloys were observed for variable Ni content. The Ni is believed to be of influence on the rate capacity because of its high catalytic activity. As the shown in Fig. 2, as the amount of Ni increases in $ZrMn_{0.5}V_{0.5}Ni_{1.4+y}$ (y=0.0, 0.2, 0.4 and 0.6) alloys, the discharge capacity decreases. However, it was unexpectedly found that the rate capability decreases with increasing Ni content in the alloys. After separating the factors affection the rate capacity into the factors related to specific reaction surface area (S) and specific surface catalytic activity, i.e., the exchange current density (i_0), it was identified that the major factor affecting the rate capability of this alloy system is the specific reaction surface area, not the specific surface catalytic activity (Fig. 3). The reaction surface area of the alloy can be changed according to its own pulverization rate related to internal stress in the alloy during charge–discharge cycles and to brittleness of the alloy itself. On the other hand, it was reported that Mn-containing alloys were too brittle so that they were easily pulverized during charge–discharge cycles [2]. Therefore, in order to identify the role of Mn in this Zr-based alloy system, the volume expansion ratio and mechanical strength of $ZrMn_{0.5}V_{0.5}Ni_{1.4+y}$ (=the Mn-rich alloy) and $ZrMn_{0.3}V_{0.7}Ni_{1.4+y}$ (=the less Mn-rich alloy) (y=0.0, 0.2, 0.4 and 0.6) were measured. From the above study, it was found that the Mn-rich system, i.e., the $ZrMn_{0.5}V_{0.5}Ni_{1.4}$ alloys, show a higher rate capability (Fig. 4) because of a larger reaction surface area due to the higher brittleness associated with the larger amount of Mn. Based on the above result, Mn is identified to be more effective in improving the rate capacity than Ni and is also known to lead to a more stable hydride than Ni [3]. Therefore, the substitution of Mn for Ni may improve the rate capacity. After determining the hydrogen storage performance and the discharge characteristics of

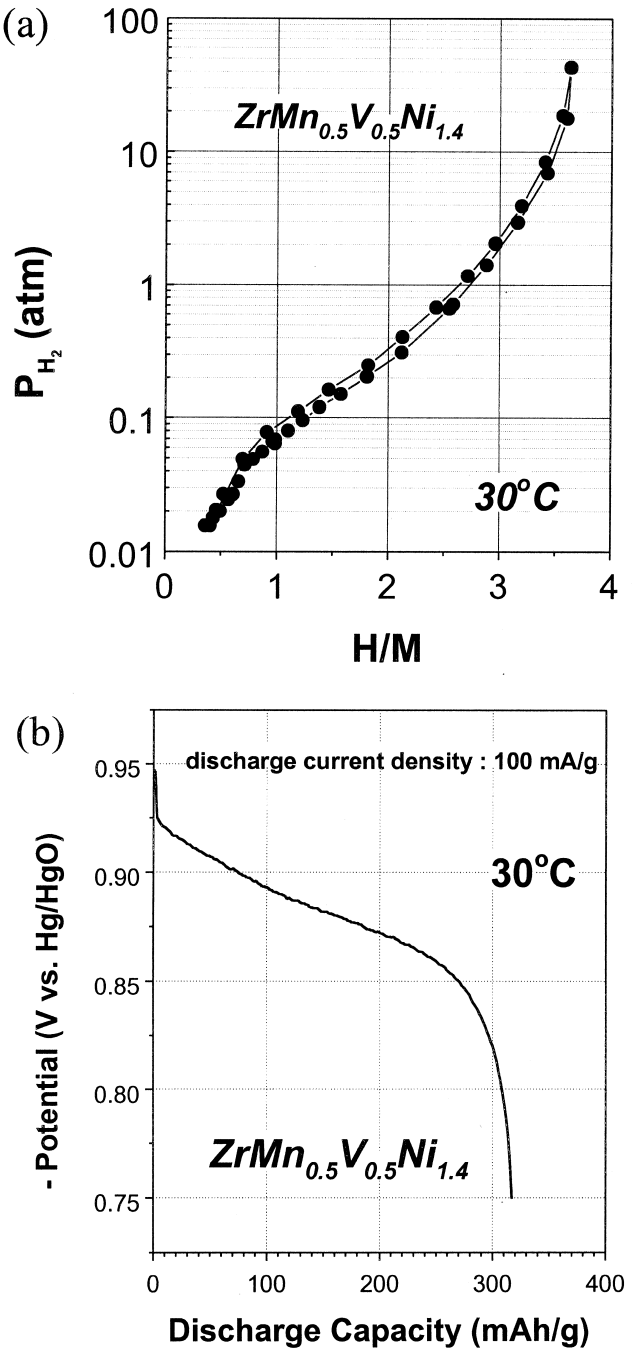

Fig. 1. (a) The PCT curves of $ZrMn_{0.5}V_{0.5}Ni_{1.4}$ alloys at 30°C; (b) The discharge current density of 100 mA g^{-1}.

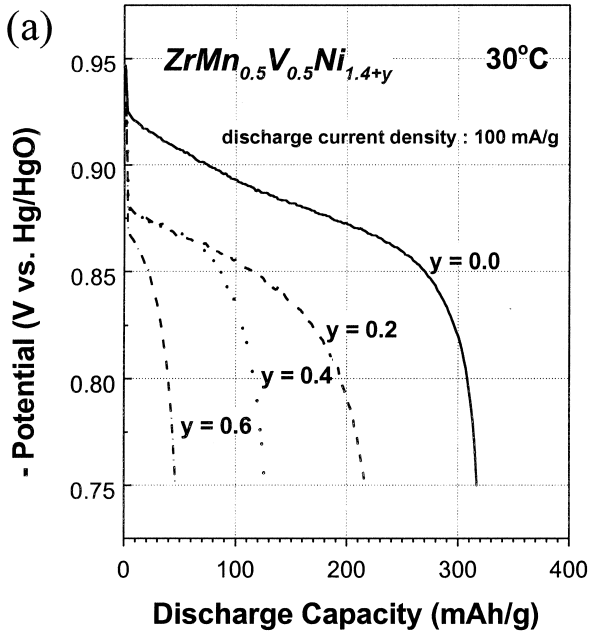

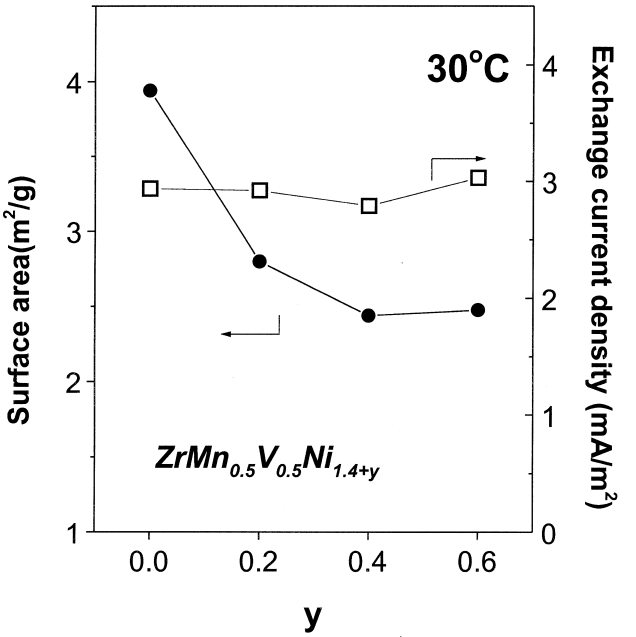

Fig. 3. Comparison of reaction surface area and exchange current density of $ZrMn_{0.5}V_{0.5}Ni_{1.4+y}$ (y=0.0, 0.2, 0.4, and 0.6) alloys at 30°C.

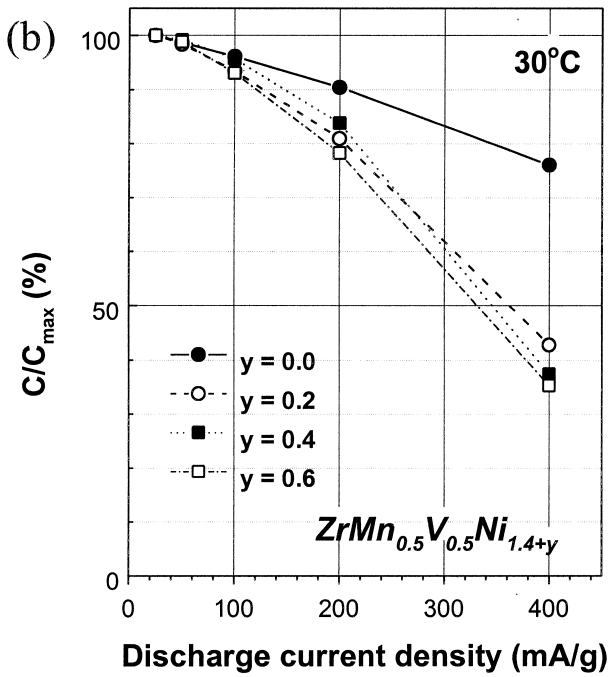

Fig. 2. (a) The discharge curves of $ZrMn_{0.5}V_{0.5}Ni_{1.4+y}$ (y=0.0, 0.2, 0.4 and 0.6) alloys at the discharge current density of 100 mA g^{-1}; (b) The rate capabilities of $ZrMn_{0.5}V_{0.5}Ni_{1.4+y}$ (y=0.0, 0.2, 0.4, and 0.6) alloys.

$ZrMn_{0.5+x}V_{0.5}Ni_{1.4-x}$ (x=0.0, 0.2 and 0.4) alloys for variable amount of substituted Mn, the alloy composition was optimized for $ZrMn_{0.7}V_{0.5}Ni_{1.2}$. This alloy show a discharge capacity of about 330 mAh g^{-1} and somewhat good rate capacity (Fig. 5).

2.3. Optimization of alloy composition for high capacity and high rate capacity

In order to improve the discharge capacity still more, Zr was partially substituted by Ti in the $ZrMn_{0.7}V_{0.5}Ni_{1.2}$ alloy. Zr in the $ZrMn_{0.7}V_{0.5}Ni$ alloy has larger atomic weight discharge capacity. After observation of discharge

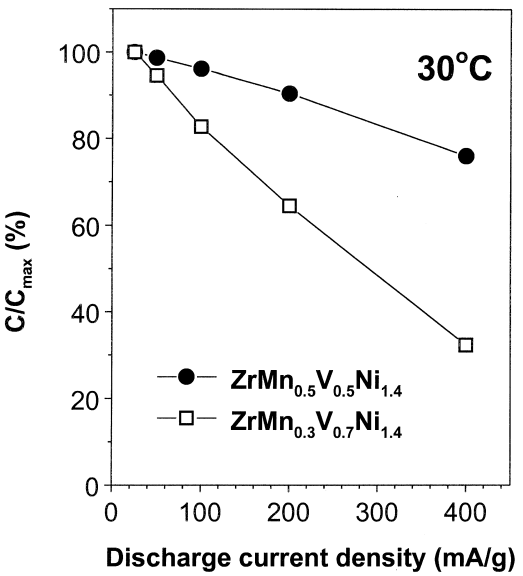

Fig. 4. Comparison of rate capability of $ZrMn_{0.5}V_{0.5}Ni_{1.4}$ and $ZrMn_{0.3}V_{0.7}Ni_{1.4}$.

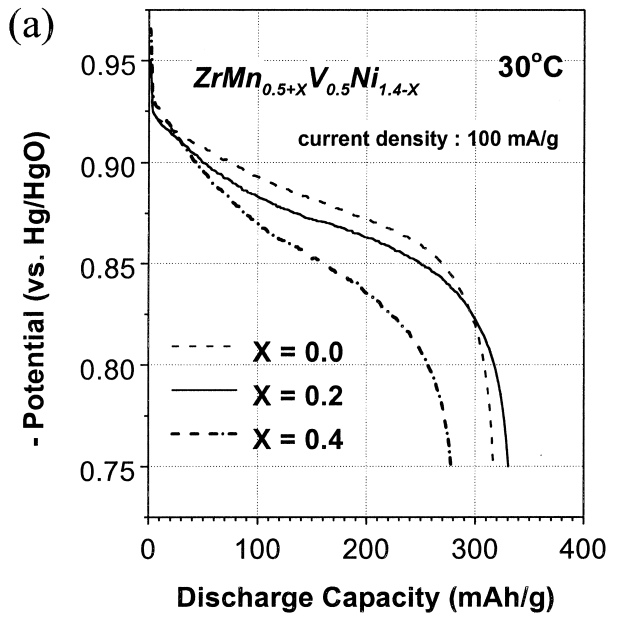

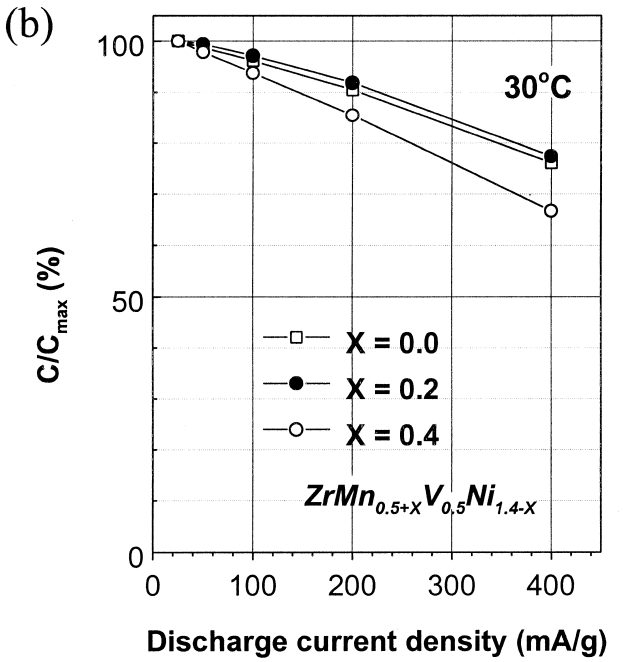

Fig. 5. (a) The discharge curves of $ZrMn_{0.5+x}V_{0.5}Ni_{1.4-x}$ (x=0.0, 0.2 and 0.4) alloys at the discharge current density of 100 mA g^{-1}; (b) The rate capacities of $ZrMn_{0.5+x}V_{0.5}Ni_{1.4-x}$ (x=0.0, 0.2 and 0.4) alloys.

capacity, it was found as shown in Fig. 6 that the electrochemical discharge capacity passes through a maximum with respect to Ti content in the alloy. In order to analyze the above phenomenon, the PCT curve measurement was performed on $Zr_{1-x}TiMn_{0.7}V_{0.5}Ni_{1.2}$ (x=0.0, 0.1, 0.15 and 0.2) alloys. From PCT curves in Fig. 7, it was observed that the hydrogen storage capacity decreases continuously and hydrogen equilibrium pressure increases

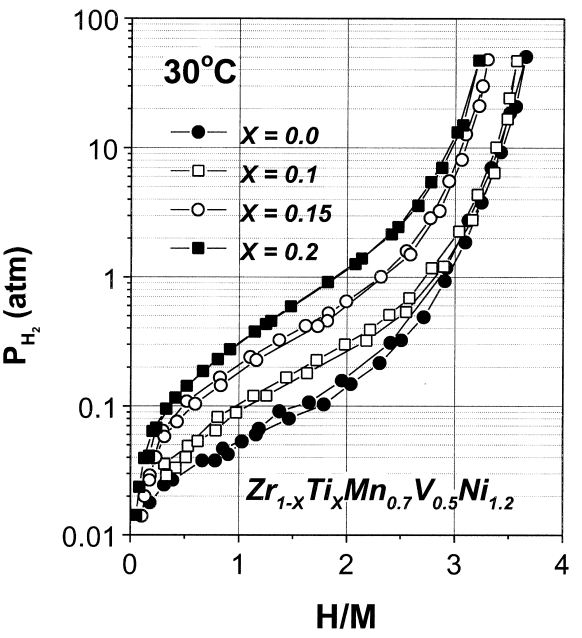

Fig. 6. PCT curves of $Zr_{1-x}Ti_xMn_{0.7}V_{0.5}Ni_{1.2}$ alloys at 30°C.

with increasing Ti content in the alloys. It seems that an increase of the hydrogen equilibrium pressure and a decrease of the amount of stored hydrogen can be attributed to the lattice shrinkage and the change of chemical affinity for hydrogen of the metals (Zr has stronger chemical affinity for hydrogen than Ti [3]). In spite of decrease of the hydrogen storage capacity with respect to Ti content, the electrochemical discharge capacity passed through a maximum with respect to the substituted Ti content in the alloy. Therefore, it is thought that there exists another factor affecting the electrochemical discharge capacity and this factor is supposed to be discharge

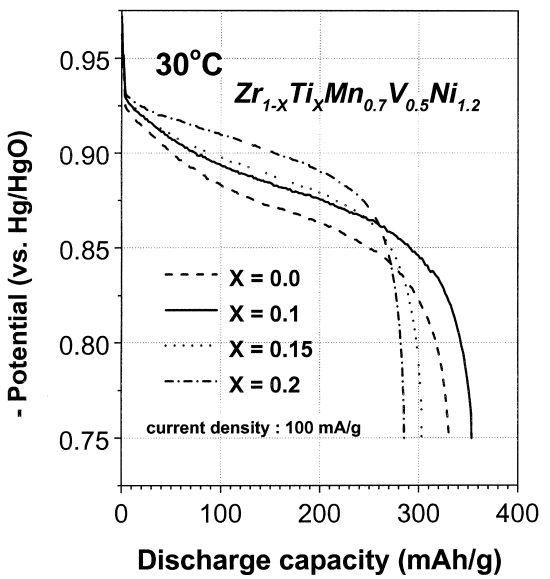

Fig. 7. Discharge capacities of $Zr_{1-x}Ti_xMn_{0.7}V_{0.5}Ni_{1.2}$ alloys.

kinetics, i.e., rate capacity. After observation of the rate capacities of $Zr_{1-x}Ti_xMn_{0.7}V_{0.5}Ni_{1.2}$ (x=0.0, 0.1, 0.15 and 0.2) alloys with respect to Ti content at 30°C, it is found that as the amount of substituted Ti increases, the rate capacity increases. The presence of a maximum point in the electrochemical discharge capacity curve of the alloys with the variable substituted Ti content is attributed to the result of the decrease of hydrogen storage capacity and the increase of rate capacity. Furthermore, the increase of the rate capacity of this alloy system with respect to increasing substituted Ti content may be due to the formation of Ti-oxide film on the MH surface, which is believed to be more porous than Zr-oxide and hydrogen penetrates more easily through this porous surface of Ti-oxide [4]. This alloy system reveals good electrochemical properties at the composition of $Zr_{0.9}Ti_{0.1}Mn_{0.7}V_{0.5}Ni_{1.2}$ which shows about 360 mAh g^{-1} of discharge capacity at the current density of 100 mA g^{-1}. The discharge efficiency, i.e., the ratio of discharge capacity at the current density of 25 mA g^{-1} to theoretical capacity calculated from PCT curves, of this alloy is identified to be as high as about 92%. Considering the discharge efficiency of $Zr_{0.9}Ti_{0.1}Mn_{0.7}V_{0.5}Ni_{1.2}$ alloy, to increase the discharge capacity of this alloy, it is necessary to increase theoretical capacity rather than to increase discharge efficiency.

Because it is generally believed that the amount of hydrogen stored reversibly in the hydrogen storage alloy only in the pressure range between about 0.01 and 5 atm at the room temperature is the useful capacity of all electrode alloys, in order to increase the theoretical capacity, the hydrogen equilibrium pressure of $Zr_{0.9}Ti_{0.1}Mn_{0.7}V_{0.5}Ni_{1.2}$ alloy should be modified by changing the stoichiometric ratio of hydride forming element part (i.e. Zr, Ti) to transition element part (i.e. Mn, V, Mn).

To adjust hydrogen equilibrium pressure of $Zr_{0.9}Ti_{0.1}Mn_{0.7}V_{0.5}Ni_{1.2}$ alloy in above mentioned pressure range, the PCT curves were measured for the $(Zr_{0.9}Ti_{0.1})(Mn_{0.7}V_{0.5}Ni_{1.2})_x$ alloys with the various stoichiometric ratios, i.e., x=1.0, 0.95, 0.92, 0.88 and 0.84. As the x value decreases, the amount of $(Mn_{0.7}V_{0.5}Ni_{1.2})$ decreases; the hydrogen equilibrium pressure also decreases, as can be seen Fig. 8.

However, the theoretical capacity passes again through a maximum with respect to x value. On the other hand, it is also shown in Fig. 8 that the rate capacity is rarely changed corresponding to the x value. Accordingly, as shown in Fig. 9, the discharge capacity is obtained at the composition of $Zr_{0.9}Ti_{0.1}(Mn_{0.7}V_{0.5}Ni_{1.2})_{0.92}$.

In this work, as shown in Fig. 10, we developed the $Zr_{0.9}Ti_{0.1}(Mn_{0.7}V_{0.5}Ni_{1.2})_{0.92}$ alloy. It has a discharge capacity of 394 mAh g^{-1} at a discharge current density of 0.25C, i.e., its capacity is higher by about 35% than that of the commercialized AB_5-type alloy, and it shows a very high rate capacity equaling that of the commercialized AB_5-type alloy.

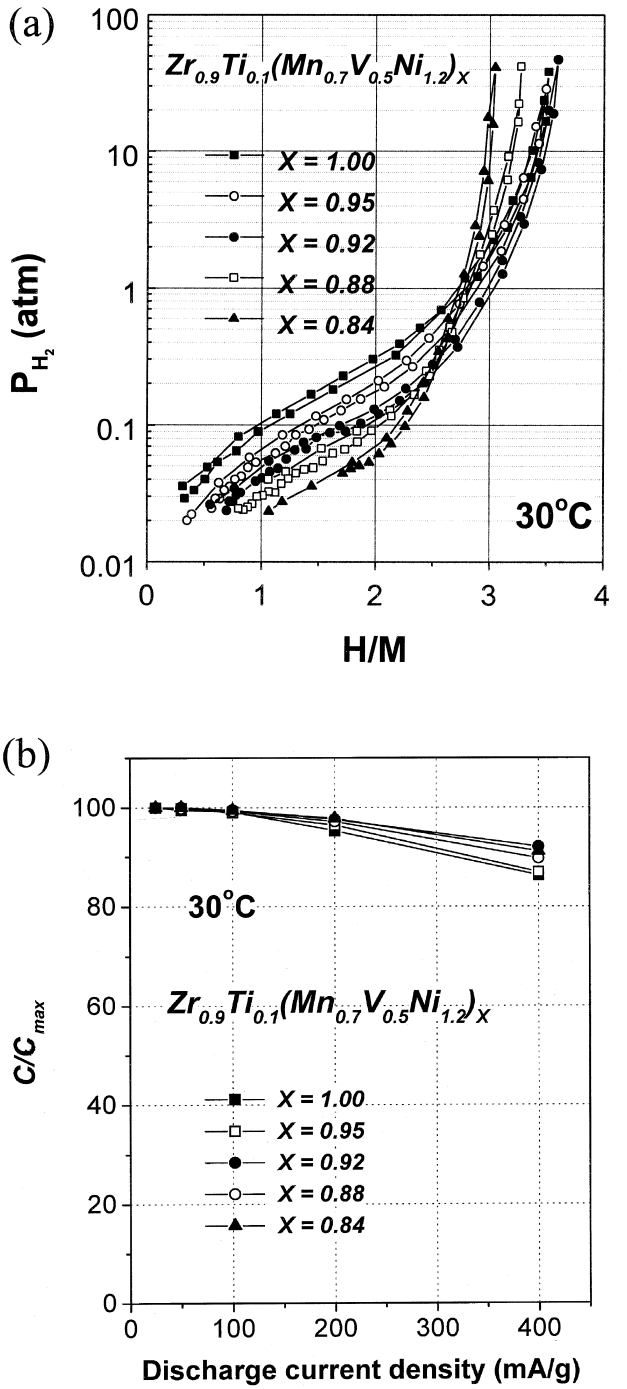

Fig. 8. (a) PCT curves and (b) rate capacities of $(Zr_{0.9}Ti_{0.1})(Mn_{0.7}V_{0.5}Ni_{1.2})_x$ (x=1.0, 0.95, 0.92, 0.88 and 0.84) alloys for variable stoichiometric ratio at 30°C.

3. Experimental details

Alloys were prepared by arc-melting of the components with a purity of more than 99.5% under argon atmosphere. Then the alloys were mechanically crushed and ground to prepare powder below 400 mesh (less than 37 μm). The crystal structure of the alloys were confirmed by X-ray

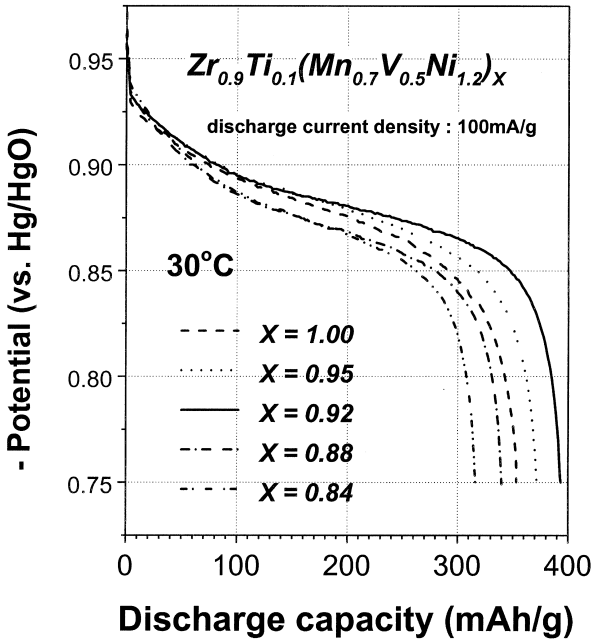

Fig. 9. Discharge curves of $(Zr_{0.9}Ti_{0.1})(Mn_{0.7}V_{0.5}Ni_{1.2})_x$ (x=1.0, 0.95, 0.92, 0.88 and 0.84) alloys with respect to stoichiometric ratio.

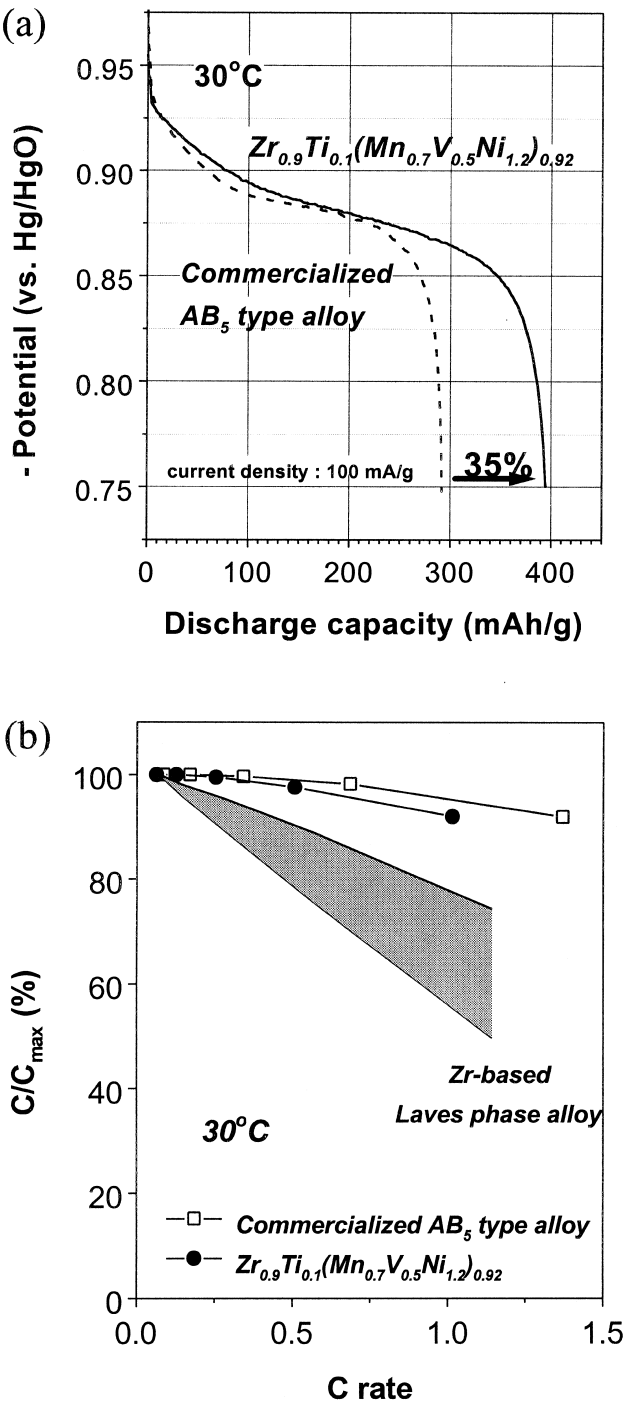

Fig. 10. (a) Discharge capacities and (b) the rate capabilities of the commercialized AB_5-type alloy and $Zr_{0.9}Ti_{0.1}(Mn_{0.7}V_{0.5}Ni_{1.2})_{0.92}$.

powder diffraction analysis. In order to investigate the hydrogen storage performance of the alloys, PCT curves were measured using an automatic Sieverts-type apparatus made by ourselves. The MH electrode was made by mixing alloy powder (less than 400 mesh) with Cu powder (about 1 μm) at a weight ratio of 1:0.25. The mixture was cold pressured to a pellet with a diameter of 10 mm and a thickness of about 1 mm at a compacting pressure of 10 ton cm^{-2}. A half-cell was constructed using a MH alloy powder electrode as a working electrode, a platinum wire as a counter electrode and a mercury/mercury oxide (Hg/HgO) electrode as a reference electrode in 30 wt.% KOH electrolyte. During the hot-charging treatment, electrodes were immersed in 30 wt.% KOH solution at controlled temperatures in the range of 50°C~80°C and charged simultaneously at charging current density in the range of 50~300 mA g^{-1} for 2~8 h. The treated electrodes were then cooled and discharged at 25 mA g^{-1} to determine a charge quantity during the hot-charging treatment. During the normal cycles, the electrode was charged with a current density of 100 mA g^{-1} of 6 h and discharged with same current density to −0.75 V vs. Hg/HgO.

Several analyses, i.e., scanning electron microscopy, AES (auger electron spectroscopy), XPS (X-ray photoelectron spectroscopy), ICPS (inductive coupled plasma spectroscopy) etc. were performed to characterize the electrode properties.

3.1. The optimization of hot-charging treatment condition and improved activation property

As shown in Fig. 11, the $Zr_{0.7}Ti_{0.3}Cr_{0.3}Mn_{0.3}V_{0.4}Ni_{1.0}$ alloy reveals good properties in view of hydrogen storage capacity of about 1.5 wt.% at hydrogen equilibrium pressure ranges of application, but this alloy has very poor activation property.

In order to optimize the hot-charging condition, the discharge of the alloy electrodes treated by the hot-charging treatment at various temperatures and charging current densities for 8 h were measured as a function of cycle number (Fig. 12). The initial discharge capacities, indicating a direct measure of electrochemical activation, increase

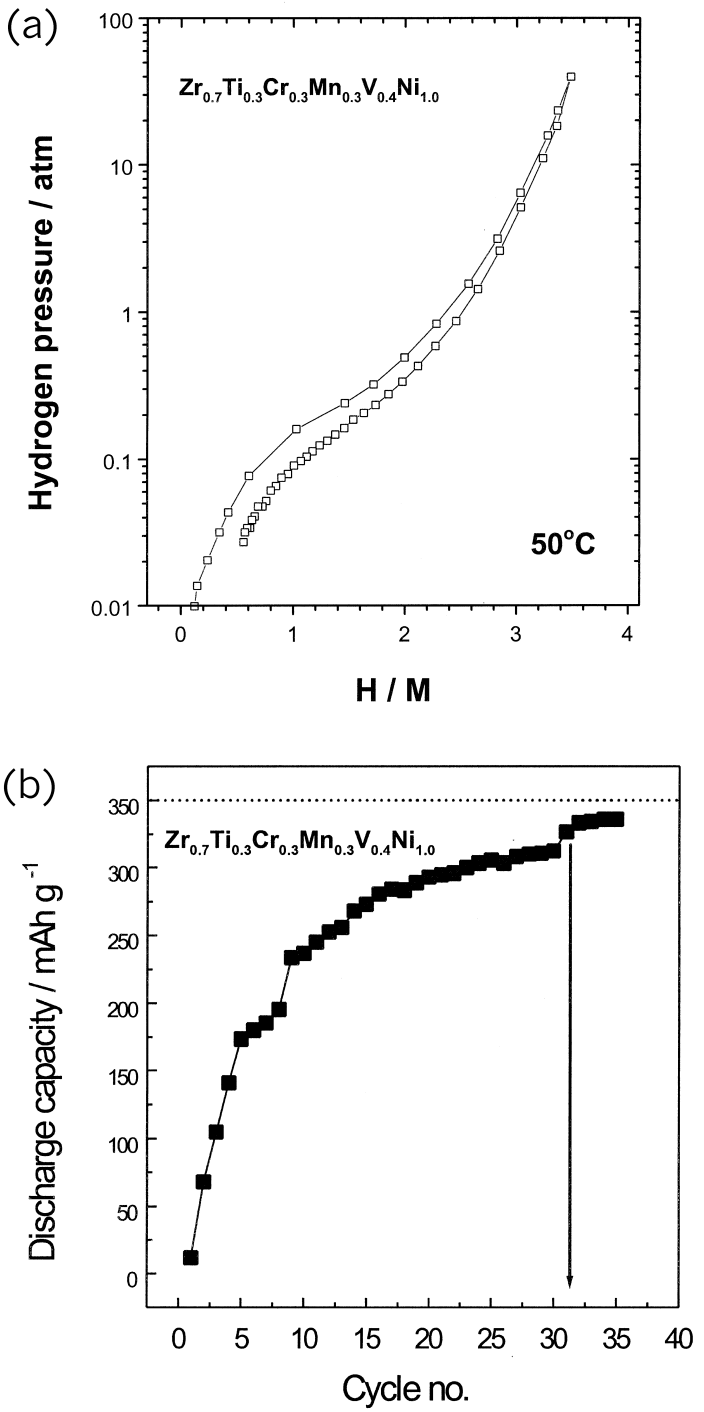

Fig. 11. (a) PCT curves of $Zr_{0.7}Ti_{0.3}Cr_{0.3}Mn_{0.3}V_{0.4}Ni_{1.0}$ alloy at 50°C and (b) its activation property.

during the hot-charging treatment. Particularly after the hot-charging treatment at 80°C and 50 mA g^{-1} for 8 h, the activation is completed after the first cycle. During the hot-charging process under the condition of 80°C and 50 mA g^{-1}, the initial discharge capacity increases gradually with treatment time and reaches the maximum discharge capacity after treatment for 8 h (Fig. 13). Therefore, it is suggested that the optimum conditions of the hot-charging treatment for easy activation of $Zr_{0.7}Ti_{0.3}Cr_{0.3}Mn_{0.3}V_{0.4}Ni_{1.0}$ alloy electrode are 80°C of solution temperature, 50 mA g^{-1} of charging current density and 8 h of treatment time, respectively.

Fig. 14 shows the variation in discharge capacity with cycle number for the electrodes untreated, treated by the hot alkaline treatment at 80°C for 8 h and treated by the hot-charging treatment at 80°C and 50 mA g^{-1} for 8 h. It was found that the untreated electrode and the electrode treated by the hot alkaline treatment are fully activated after 30 cycles and 20 cycles, respectively. However, the hot-charging treated electrode shows a high discharge

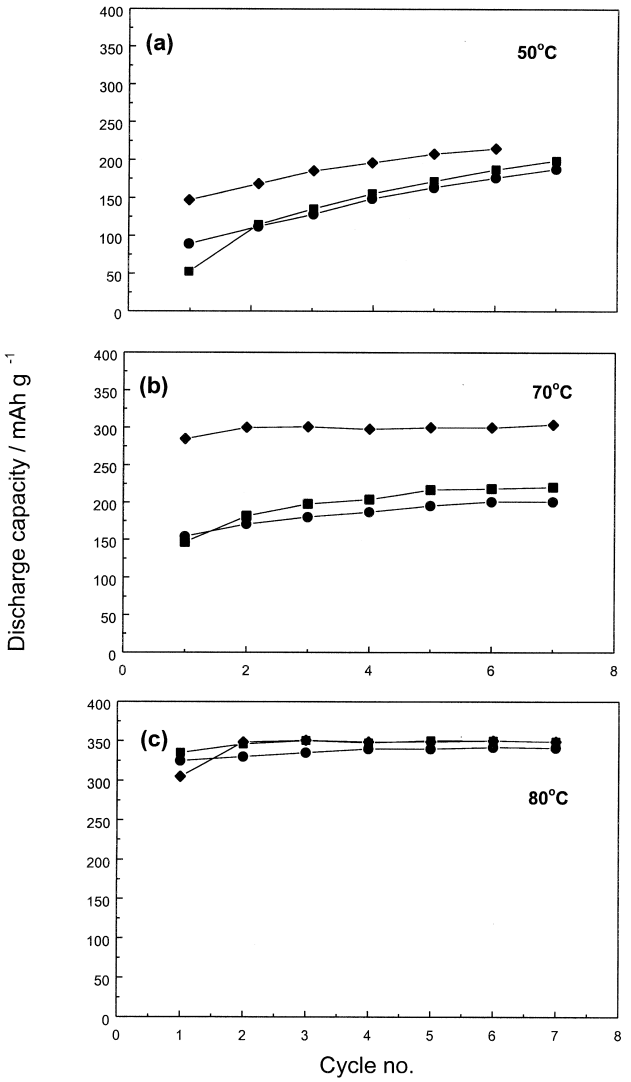

Fig. 12. Discharge capacities of alloy electrodes treated by the hot-charge process at (a) 50°C, (b) 70°C and 80°C with various charging current densities of the cycle number: (■) 50 mA/g; (●): 150 mA/g; (♦) 300 mA/g. The charge–discharge cycle test was performed at 50 mA/g.

capacity of approximately 350 mAh g^{-1} even at the first cycle. From the above results, it is concluded that the charging as well as the solution temperature plays a key role in the easy activation.

3.2. The effects of hot-charging treatment on the surface of the Zr–Ti–Cr–Mn–V–Ni alloy electrode

First, in order to explain the effects of the charging current density on activation property, the initial discharge capacity (C_0) charged during the hot-charging process for 8 h was measured (Fig. 15). C_0 increases with charging current density at a controlled temperature of 50°C. At other temperatures, the same trend is observed and C_0 is significantly greater at higher temperatures and higher charging currents. Fig. 16 shows that X-ray diffraction (XRD) patterns are shifted to lower angles. This is

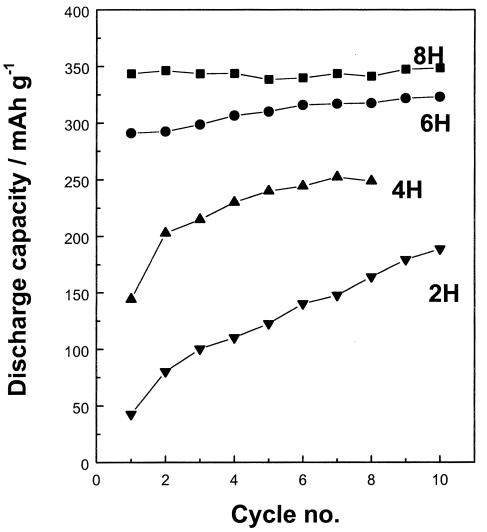

Fig. 13. Effect of the treatment time during the hot-charging treatment under the condition of 80°C and 50 mA g^{-1} on the activation behavior of $Zr_{0.7}Ti_{0.3}Cr_{0.3}Mn_{0.3}V_{0.4}Ni_{1.0}$ alloy electrode: (a) 2 h, (b) 4 h, (c) 6 h, (d) 8 h.

ascribed to the lattice expansion induced formation of cracks on the alloy surface. Therefore it is suggested that the volume expansion by a large C_0 during the hot-charging process results in the pulverization of the alloy particles and the formation of a new clean surface having a high catalytic, which improves the activation behavior of treated electrodes.

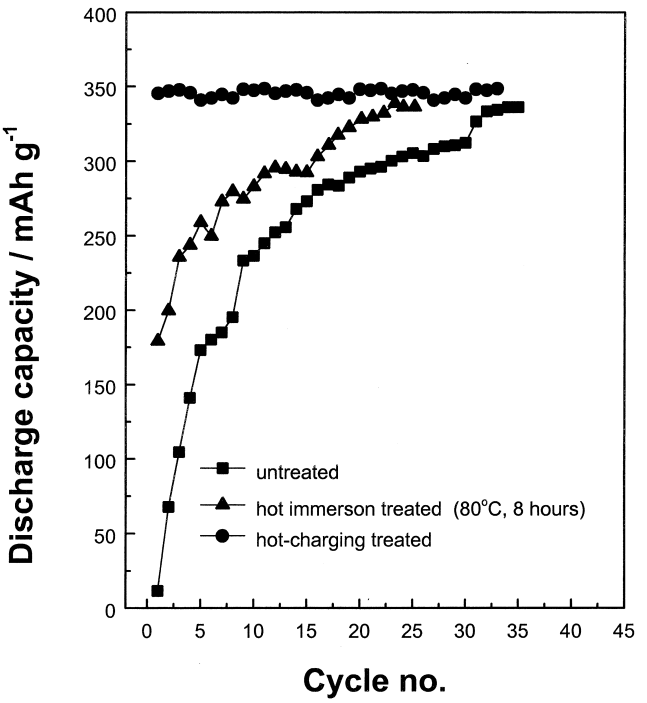

Fig. 14. Discharge capacities of the untreated alloy electrode and those treated by the hot alkaline treatment at 80°C for 8 h and treated by hot-charging treatment at 80°C and 50 mA g^{-1} for 8 h. The charge–discharge cycle test was performed at 50 mA g^{-1}.

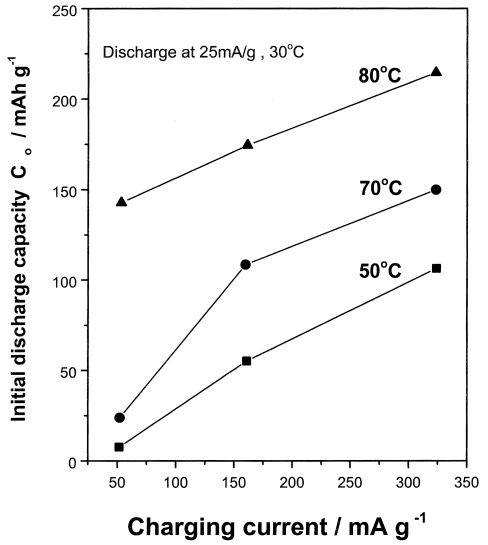

Fig. 15. Effect of the solution temperature and charging current density during the hot-charging treatment for 8 h on the initial discharge capacity, C_0, for $Zr_{0.7}Ti_{0.3}Cr_{0.3}Mn_{0.3}V_{0.4}Ni_{1.0}$ alloy electrode; 50°C, 70°C and 80°C.

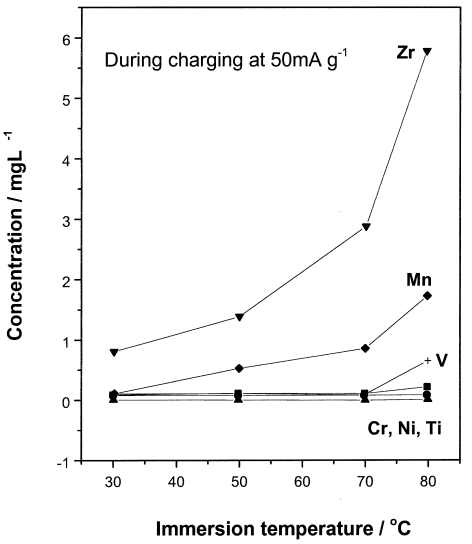

Fig. 17. Effect of the temperature treatment on the ionic concentration in the treatment solution during the hot-charging treatment with various temperature for 8 h, by ICPS.

Second, in order to explain the effects of temperature on activation property during the treatment, ICPS analysis of the electrolyte after the hot-charging treatment was performed (Fig. 17). These results show that partial dissolution of alloy components occurs during the hot-charging treatment and increases at higher temperatures. For investigating the effects of the hot-charging treatment on the surface of the alloy electrode, AES and XPS analyses were performed. The AES depth profiles for the constituent elements of the hot alkaline treated and the hot-charging treated electrodes are significantly decreased, which is consistent with the results of ICPS analysis. It is well known that these results are ascribed to the easy dissolution of their oxides [5,6]. The contents of oxygen on the subsurface layer is higher in hot alkaline treated electrodes than in the hot-charging treated electrodes, while Ni is enriched on the surface of the hot charging treated electrode. We also confirm by means of ZrO_2, TiO_2, and Ni oxide, as reported by Go et al. [7]. These oxides exist as oxide states only near the top surface, but mainly as metallic state in the subsurface with metallic Ni. This metallic Ni could allow for the excellent electrocatalytic as found in the work of Züttel et al. [5].

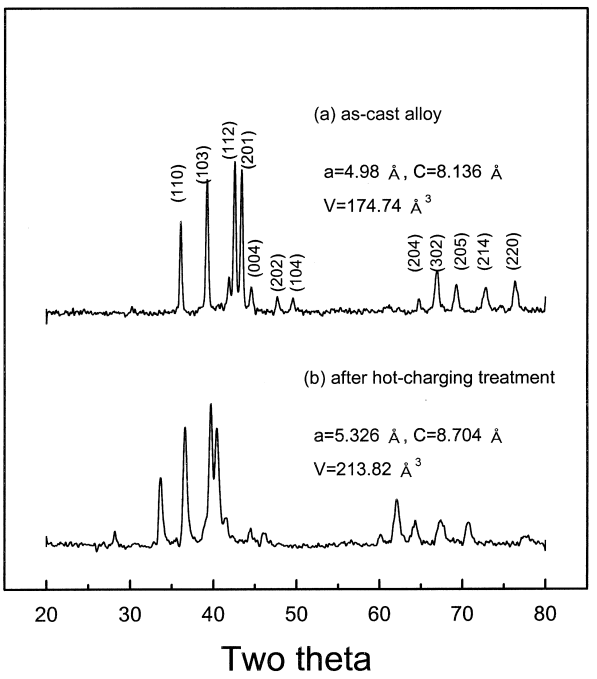

Fig. 16. XRD patterns of $Zr_{0.7}Ti_{0.3}Cr_{0.3}Mn_{0.3}V_{0.4}Ni_{1.0}$ alloy electrodes before (a) and after (b) the hot-charging treatment.

3.3. The reason for good activation property of hot-charging treated electrode

In order to explain the reason for the difference in chemical states on the surface between the hot alkaline treated electrode and the hot-charging treated electrode, the potentials of both electrodes were monitored during the treatment (Fig. 18). The potential of the electrode modified by the hot alkaline treatment is shifted in the negative direction to −0.57 V vs. Hg/HgO while the potential of the electrode modified by the hot-charging treatment is shifted in the negative direction by up to −0.9 V. Such a more negative shift of the potential during the hot-charging treatment would result in formation of a reductive atmosphere for alloy components of the electrode surface [8]. So the alloy components on the top surface as well as the subsurface could exist as the metallic state rather than the oxide state, as found in the AES and XPS analyses.

It is suggested that because the hot-charging treatment

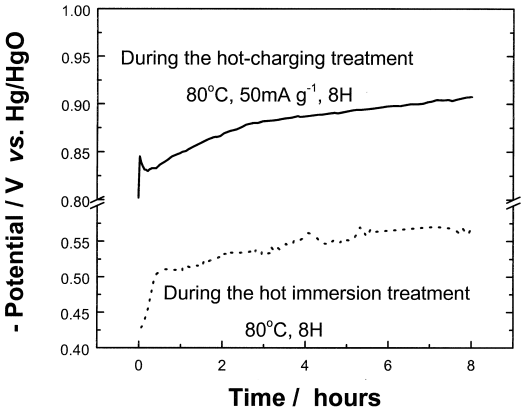

Fig. 18. The potentials of alloy electrode during (a) the hot alkaline treatment (80°C and 8 h) and (b) the hot-charging treatment (80°C, 50 mA g^{-1} and 8 h).

of electrode resulted not only in the formation of a new surface by volume expansion but also in the formation of an Ni enriched region on the surface by partial dissolution of the constituent elements and formation of a reductive atmosphere by the potential shift the negative direction, the activation property of the $Zr_{0.7}Ti_{0.3}Cr_{0.3}Mn_{0.3}V_{0.4}Ni_{1.0}$ electrode was greatly improved.

4. Conclusions

For developing Zr-based hydrogen storage alloy with a very high rate capability as well as high capacity, $ZrMn_{0.5}V_{0.5}Ni_{1.4}$ alloy as a starting material was modified through varying the stoichiometry, and finally $Zr_{0.9}Ti_{0.1}(Mn_{0.7}V_{0.5}Ni_{1.4})_{0.92}$ alloys with high capacity and high rate discharge current density of 0.25C and showing very high rate capacity equivalent to that of commercialized AB_5-type alloys were developed.

We have found that the activation behavior of the AB_2-type $Zr_{0.7}Ti_{0.3}Cr_{0.3}Mn_{0.3}V_{0.4}Ni_{1.0}$ alloy electrode is improved by immersing the electrode in hot alkaline solution and charging simultaneously (the hot-charging treatment). During this treatment, the charging of the alloy with atomic hydrogen occurs rapidly, which results in the formation of cracks and a new clean surface. Furthermore, Ni with high catalytic activity is enriched near the surface by dissolving the surface oxide layer and the new surface with Ni layer exists as the metallic state because of reductive atmosphere induced by the potential shift to the more negative region. Owing to the mentioned effects, the $Zr_{0.7}Ti_{0.3}Cr_{0.3}Mn_{0.3}V_{0.4}Ni_{1.0}$ alloy electrode treated at 80°C and 50 mA g^{-1} for 8 h is fully activated even the first cycle.

References

[1] D.M. Kim, J.H. Jung, K.J. Jang, J.Y. Lee, J. Electrochem. Soc. 145 (1) (1998) 93–98.
[2] T. Sakai, H. Miyamura, N. Kuriyama, H. Ishikawa, I. Uchida, Z. Phys. Chem. Bd. 183 (1994) S333–346.
[3] L. Schlapbach, in: Hydrogen in Intermetallic Compounds, Vol. I, Springer-Verlag, Berlin Heidelberg New York, 1988, pp. 266–273.
[4] Züttel, F. Meli, L. Schlapbach, J. Alloys Comp. 231 (1995) 645–649.
[5] Züttel, F. Mei, L. Schlapbach, J. Alloys Comp. 209 (1994) 99.
[6] F.A. Cotton, G. Wilkinson, in: Advanced Inorganic Chemistry, 3rd ed., Wiley, 1972, p. 822.
[7] X.P. Go, W. Zhang, H.B. Yang, D.Y. Song, Y.S. Zhang, Z.X. Zhou, P.W. Shen, J. Alloys Comp. 235 (1996) 225.
[8] M. Matsuoka, K. Asai, H. Asai, Y. Fukumoto, C. Iwakura, J. Alloys Comp. 192 (1993) 149.